PCCP

PAPER

View Article Online
View Journal | View Issue

Open Access Article. Published on 06 June 2023. Downloaded on 1/14/2026 1:25:04 AM.
This article is licensed under a Creative Commons Attribution-NonCommercial 3.0 Unported Licence.

Check for updates

Cite this: *Phys. Chem. Chem. Phys.*, 2023, **25**, 16273

Membrane plasticity induced by *myo*-inositol derived archaeal lipids: chemical synthesis and biophysical characterization†

Johal Ruiz,‡[a] Josephine G. LoRicco,‡[b] Laurent Soulère,[a] Marta Salvador Castell,[b] Axelle Grélard,[cd] Brice Kauffmann,[d] Erick J. Dufourc,[cd] Bruno Demé,[e] Florence Popowycz[a] and Judith Peters *[efg]

Received 11th April 2023,
Accepted 6th June 2023

DOI: 10.1039/d3cp01646c

rsc.li/pccp

Archaeal membrane lipids have specific structures that allow Archaea to withstand extreme conditions of temperature and pressure. In order to understand the molecular parameters that govern such resistance, the synthesis of 1,2-di-*O*-phytanyl-*sn*-*glycero*-3-phosphoinositol (DoPhPI), an archaeal lipid derived from *myo*-inositol, is reported. Benzyl protected *myo*-inositol was first prepared and then transformed to phosphodiester derivatives using a phosphoramidite based-coupling reaction with archaeol. Aqueous dispersions of DoPhPI alone or mixed with DoPhPC can be extruded and form small unilamellar vesicles, as detected by DLS. Neutron, SAXS, and solid-state NMR demonstrated that the water dispersions could form a lamellar phase at room temperature that then evolves into cubic and hexagonal phases with increasing temperature. Phytanyl chains were also found to impart remarkable and nearly constant dynamics to the bilayer over wide temperature ranges. All these new properties of archaeal lipids are proposed as providers of plasticity and thus means for the archaeal membrane to resist extreme conditions.

Introduction

Cell membrane structuration relies on the ability of amphiphilic molecules, containing a hydrophobic core and a hydrophilic polar head group, to self-assemble into bilayers in an aqueous environment. These structures, which probably led to the formation of the first primitive cells, are not very stable or sufficiently impermeable at the high temperatures which would have been found on the early Earth. In Archaea, it is widely acknowledged that membrane-spanning lipids, *e.g.* tetraether lipids, harbouring two polar head groups that form monolayer membranes, are a key adaptation for hyperthermophilic membranes to withstand extreme thermal or pH conditions.[2–4] Curiously, the archaeon *Thermococcus barophilus* as well as other hyperthermophilic Archaea from different groups, capable of growth above 100 °C,[5] may produce a majority of, if not exclusively, diether lipids, harbouring a single polar head group and capable of forming the more classical bilayer membrane architecture (Fig. S1, ESI†).[6]

The identity of the polar head may play an important role in the ability of diether lipids to form stable membrane bilayers at high temperature. Many studies rely on lipids with a phosphocholine (PC) head group, however, this head group is not typically found in the membranes of Archaea, in favor of various other phospholipids and glycolipids. The exact polar head groups seen in Archaea differ significantly between Families and Genera.[5,7] Additionally, the composition of the polar head groups is known to change under different growth conditions but has not been well-documented.[8] The number and diversity of polar head groups that have been detected in Archaea is quite high and due to limitations in current methodologies used in lipid extraction and characterization,[9] there are likely many head groups that have yet to be identified. Changes in lipid polar head group composition help the membrane remain in a functional state by maintaining the proper

[a] Univ Lyon, INSA Lyon, Université Claude Bernard Lyon 1, CPE Lyon, UMR 5246, CNRS, ICBMS, Institut de Chimie et de Biochimie Moléculaires et Supramoléculaires, Bât. E. Lederer, 1 Rue Victor Grignard, F-69622 Villeurbanne, France
[b] Université de Lyon, INSA Lyon, CNRS, UMR, 5240, Villeurbanne, France
[c] Univ. Bordeaux, CNRS, Bordeaux INP, CBMN, UMR 5248, F-33600 Pessac, France
[d] Institut Européen de Chimie et Biologie, CNRS, Université de Bordeaux, INSERM, UAR3033, France
[e] Institut Laue-Langevin, 38000 Grenoble, France. E-mail: jpeters@ill.fr
[f] Univ. Grenoble Alpes, LiPhy, CNRS, 38000 Grenoble, France
[g] Institut Universitaire de France, France

† Electronic supplementary information (ESI) available: Schematic representation of (A) bipolar tetraether lipids, (B) monopolar diether lipids. (C) Molecular target (1,2-di-*O*-phytanyl-*sn*-*glycero*-3-phosphatidylinositol); synthesis strategy of phosphatidylserine and phosphatidylglycerol derivatives of archaeol; sample preparation for synthesis; protocols related to organic syntheses; supplementary DLS data; supplementary neutron data; supplementary NMR and SAXS data. See DOI: https://doi.org/10.1039/d3cp01646c

‡ Both authors contributed equally.

Open Access Article. Published on 06 June 2023. Downloaded on 1/14/2026 1:25:04 AM. This article is licensed under a Creative Commons Attribution-NonCommercial 3.0 Unported Licence.

membrane parameters such as fluidity and permeability under "extreme" conditions.

Hyperthermophiles are capable of producing lipids with many diverse head groups. The phosphoinositol (PI) head group is found commonly throughout the Archaea domain including many hyperthermophilic species. For example, those belonging to the Thermococcales order are known to produce a high proportion of PI lipid (up to 98%)[10] (*Pyrococcus furiosus*, *Pyrococcus yayanosii* and *Thermococcus kodakarensis*, *Methanopyrus kandleri*, *Methanothermus fervidus*, and *Sulfolobus acidocalaruis*). In order to test whether certain head groups are responsible for the stability of archaeal lipids membranes under high temperature conditions we first needed to synthesize these lipids.

The first part of this article reports the synthesis of a *myo*-inositol derived archaeal lipid, 1,2-di-*O*-phytanyl-*sn-glycero*-3-phosphatidylinositol (DoPhPI), as a possible component of monopolar/diether Archaea cell membranes. The monopolar archaeal core lipids could be obtained from the commercially available phytol on which the appropriate polar head groups can be later grafted. In addition, lipids of different size and polarity could be synthesized in order to generate lipids of divergent properties and decipher their impact on membrane structure and stability.

Further, we present the study of the assembled structure and dynamics of different archaeal lipids, namely 1,2-di-*O*-phytanyl-*sn-glycero*-3-phosphatidylcholine (DoPhPC) and DoPhPI, as dispersions and mixtures in excess water, *i.e.*, for 80–85% hydration representing *ca.* 200 water molecules per lipid, a situation representative of concentrations found in nature.

We used a combination of different techniques in order to assess the structure and dynamics of the assembled archaeal lipid membranes including:

– Dynamic Light Scattering (DLS), which allows the determination of the diffusion coefficient and hydrodynamic radius of vesicles in solution.

– Neutron diffraction, which allows the determination of the lamellar *d*-spacing of the membranes as a function of temperature and pressure.

– Solid state nuclear magnetic resonance (ssNMR) with observation of deuterium (^{2}H), phosphorus (^{31}P) and carbon (^{13}C). Wide line (static) ssNMR provides the nature of the lipid phases. ^{2}H-NMR is obtained using probe amounts of chain deuterated DPPC as a reporter for lipid phases and internal chain dynamics. Rotating the sample at the magic angle (MAS) and use of different polarization transfer (PT) schemes provides high resolution spectra and specific dynamic information on phytanyl chains and head groups. NMR is complemented by Wide/Small-Angle X-rays scattering (WAXS/SAXS) on the same samples to ascertain lipid phases found by ssNMR.

Materials and methods

Chemicals

DoPhPC and 1-palmitoyl-2-($^2H_{31}$)palmitoyl-*sn-glycero*-3-phosphocholine ($^2H_{31}$-DPPC) were bought from Avanti Polar Lipids (Alabaster, USA) in the lyophilized form and utilized without further purification. Purity was guaranteed >99%. Chloroform ($CHCl_3$) and the deuterium-depleted water were purchased from Sigma Aldrich (Saint-Quentin Fallavier, France) and 4 mm (100 μL) ZrO_2 rotors and caps from Cortecnet (Les Ulis, France).

The 1,2-di-*O*-phytanyl-*sn-glycero*-3-phosphatidylinositol (DoPhPI) was synthesized as described in the "Chemical Synthesis" portion of the Results section.

Sample preparation

(i). For DLS: vesicle preparation. Lipid films with the desired lipid compositions were formed by dissolving the lipids in 2 : 1 chloroform : methanol and then allowing the solvent to evaporate. Films were placed under vacuum overnight to ensure complete evaporation of solvent. The lipid films were then hydrated by addition of 50 mM Tris pH 7.4 D_2O, so that the final lipid concentration was 10 mg mL^{-1} (12 mM followed by vigorous vortexing to form multilamellar vesicles (MLVs), followed by 5 cycles of freeze/thaw with vortexing between cycles. MLVs were then passed through a 0.1 μm polycarbonate membrane 11× using the Avanti mini-extruder at 45 °C to form unilamellar vesicles (ULVs).

(ii). For neutron diffraction experiments. Lipid bilayers were studied as a multistack of hundreds of lipid bilayers on a substrate to enhance the intensity of the scattered neutrons. The substrates used were one-side polished ultraclean silicon wafers with a thickness of 275 ± 25 μm purchased from Si-Mat (Germany). Si wafers were rinsed with ethanol and dried by a nitrogen flux. The wafers were previously cut to fit the sample compartment of the flat aluminium cells or the high-pressure cell.

For the flat aluminum cells, we deposited 3 mg of lipid on a single wafer and sealed the cell with 50 μL of the correct D_2O contrast. The temperature (up to 85 °C) could be controlled with an orange cryostat, in which the sample stick was stuck.

(iii). For NMR and SAXS experiments. Samples were prepared by dissolving in chloroform DPPC, DoPhPC and equimolar quantities of DoPhPI. 10 mol% $^2H_{31}$-DPPC was also added in all samples. The chloroform was evaporated under a stream of nitrogen. The residual lipid film was dispersed in 1 mL of milliQ filtered water and freeze-dried overnight to remove all traces of chloroform. The resulting powder (*ca.* 20 mg) was suspended into 100 μL of deuterium-depleted water to obtain a hydration, h, of 80 to 85% (h = mass of water over the total mass of the system (phospholipids + water)). After shaking into a vortex mixer, samples were frozen in liquid nitrogen for 30 s, heated at 55 °C for 10 min in a water bath and shaken again for better sample homogeneity; this freeze–thaw–shaking cycle was repeated 3 times and the resulting milky dispersion transferred into a 4 mm diameter Zirconium dioxide rotor.

The same samples were used for SAXS experiments.

Experimental setups

(i). DLS experiments. DLS measurements were made simultaneously with spin echo measurements using the *in situ* DLS

 This journal is © the Owner Societies 2023

Open Access Article. Published on 06 June 2023. Downloaded on 1/14/2026 1:25:04 AM.
This article is licensed under a Creative Commons Attribution-NonCommercial 3.0 Unported Licence.

device on IN15[11,12] (ILL, Grenoble). The ILL data is available at 10.5291/ILL-DATA.8-02-898. The autocorrelation function was fit using the following method of cumulants:[13]

$$g^2(\tau) = 1 + \beta \times \exp(-2\Gamma\tau) \times \left(1 + \frac{\mu_2}{2}\tau^2\right)^2 \quad (1)$$

where β is a scaling factor that depends on the sample geometry, Γ is the rate of decay, τ is the correlation time and μ_2 is the first moment about the mean corresponding to the variance. The diffusion coefficient (D) can be determined from the relationship, $\Gamma = Dq^2$ where the scattering vector (q) is defined by: $q = 4\pi n/\lambda_\text{HeNe}\sin(\theta/2)$. The refractive index $n = 1.33$, the wavelength of the HeNe laser = 632.8 nm, and the scattering angle $\theta = 90°$. The hydrodynamics radius (R_h) can then be determined through the Stokes–Einstein relationship,

$$R_h = \frac{k_B T}{6\pi \times \eta(T) \times D} \quad (2)$$

where k_B is the Boltzmann constant, T is the temperature, $\eta(T)$ is the viscosity of the solvent. The polydispersity index PDI = μ_2/Γ^2.

(ii). Neutron diffraction experiments. Neutron diffraction experiments were performed on multistacks of oriented membrane bilayers on the D16 small momentum transfer diffractometer[14] at the Institut Laue Langevin (France) using the incident wavelength $\lambda = 4.55$ Å, and an accessible q-range from 0.06 Å^{-1} to 0.51 Å^{-1}. The scattering wave vector q is defined as:

$$q = 4\pi \sin(\theta)/\lambda \quad (3)$$

where 2θ is the scattering angle. The wafer with the sample was or placed inside a cylindrical high pressure cell[15] and the high-pressure sample stick[16] or in a flat Al sample holder. The Si wafer was positioned vertically parallel to the neutron beam so that the multistack of lipid bilayers on its surface was also parallel to the beam, and its angle, *i.e.* Ω, was rotated from $-1°$ to 12° by 0.05° steps. The detector was placed at $\Gamma = 12°$ from the sample. The ILL data is available at 10.5291/ILL-DATA.8-02-919 and 10.5291/ILL-DATA.8-02-951.

The lamellar d-spacing of the lipid bilayer was determined from the observed scattering angles 2θ of the Bragg peak positions according to $d = 2\pi/q$. For the data analysis, we used the software Origin (OriginPro, Version 2016. OriginLab Corporation, Northampton, MA, USA).

Neutron scattering length density (NSLD) profiles were constructed using the following equation:

$$\rho(z) = \frac{2}{d}\sum_{h=1}^{h_{\max}} |F_h| v_n \cos\left(\frac{2\pi h}{d}\right) z, \quad (4)$$

where d is the lamellar spacing of the bilayer in the z direction, $z \in [-d/2, d/2]$, $|F_h| = \pm\sqrt{I_h Q_h}$, Q_h is the Lorentz correction factor equal to q for oriented bilayers, I_h is the integrated intensity of the hth Bragg peak and v_n is the phase of the structure factor, corresponding to [−1,−1, + 1, −1].

For the determination of the membrane lateral spacing, the location of peaks along the Ω-axis was determined. The data was reduced to intensity *vs.* Ω plots for several values of 2θ. Gaussian fits were then used to determine the center of the satellite peaks. Numbering of the satellite peak order along the q_x axis (h) began at $\Omega = 2.45°$ corresponding to $h = 1$. The angle between the peaks ($\Delta\Omega$) was determined by plotting the peak locations as a function of peak order. The scattering vector q was then determined using eqn (3) where θ in this case is the half angle between the two omega peaks. The repeating distance in the membrane plane (d_x) was calculated by $d_x = 2\pi/q$.

(iii). NMR experiments. Solid-state ^{31}P and ^{2}H NMR were performed on a Bruker NEO 800 MHz SB spectrometer (Bruker Biospin, France) equipped with a triple ^{1}H/^{2}H/^{31}P 4 mm MAS probe. ^{31}P-NMR spectra were acquired at 323.94 MHz by using a proton decoupled Hahn-echo pulse sequence.[17] Typical acquisition parameters were as follows: spectral window of 96 kHz, π/2 pulse width of 4.64 μs, interpulse delay of 40 μs and recycle delay of 5 s. Typically 500 scans were accumulated. ^{2}H-NMR spectra were acquired at 122.84 MHz by means of a quadrupolar echo pulse sequence,[18] with a spectral width of 500 kHz, a π/2 pulse width of 4.7 μs, a 40 μs interpulse delay and a recycle delay of 2 s. Typically, 1k scans were recorded depending on temperature. A Lorentzian noise filtering of 100 and 200 Hz, for ^{31}P and ^{2}H respectively, was applied prior Fourier transformation from the top of the echo signal. Samples were allowed to equilibrate at least 20 min at a given temperature before the NMR signal was acquired.

Magic angle sample spinning (MAS) and Cross Polarization (CP),[19] Insensitive Nuclei Enhanced by Polarization Transfer (INEPT)[20] and Direct Polarization (DP) experiments were accomplished for carbon detection. A spinning rate of 11 kHz and temperature stabilization at 20 °C was applied for experiments. Acquisitions were performed on a Bruker Avance III 500 MHz WB spectrometer equipped with a dual H/X MAS probe. A ramped CP with 1 ms contact time was used for the ^{1}H–^{13}C polarization, 100 kHz proton high-power decoupling, using the SPINAL-64 decoupling sequence, was applied during the 20 ms acquisition time and 2 k scans were acquired with a recycle delay of 5 s for CP, INEPT and DP sequences. A Lorentzian noise filtering of 30 Hz was applied prior Fourier transformation.

Spectral simulations. Wide-line ssNMR spectra were simulated in the time domain and then Fourier transformed. Individual components are constructed from experimental estimates of chemical shielding anisotropies ($\Delta\sigma$) or quadrupolar splittings ($\Delta\nu_Q$), isotropic chemical shifts and individual line widths. Small variations are allowed to match with sharp experimental features on spectra and comparison between experimental and calculated spectra is made until a satisfactory superimposition is obtained. For lipids containing perdeuterated chains, weights for individual C–^{2}H$_2$ or C–^{2}H$_3$ are determined from the number of deuterons per labelled carbon position; the individual time dependent signals are then added accordingly leading after Fourier transformation to the multicomponent spectrum. Such a simulation leads to individual quadrupolar splittings, $\Delta\nu_Q^k$, for labelled carbon positions, k, and subsequently to S_{CD}^k order parameters in bilayer membranes.[21] The simulation also implements partial orientation/deformation of vesicles, tubes, bicelles, *etc.*, using the theory developed by Pott

Open Access Article. Published on 06 June 2023. Downloaded on 1/14/2026 1:25:04 AM.
This article is licensed under a Creative Commons Attribution-NonCommercial 3.0 Unported Licence.

and Dufourc.[22] The simulation program for wide line spectra has been developed in FORTRAN and implemented in a user-friendly graphical interface (Microsoft.NET) for Windows platforms. The program is available on demand.

Calculation of spectral moments and chain length. For wide-line solid-state ^{2}H-NMR and when the spectrum is composed of a single lamellar phase, spectral moments allow to quantitate thermally-induced spectral changes and were calculated according to Beck *et al.*[1] and Davis[23] using a FORTRAN code implemented in a user-friendly routine, NMRFriend, by Buchoux *et al.*[24] Calculation of deuterated chain length is performed according to Douliez *et al.*[25] by making use of the S^k_{CD} order parameters obtained from simulations. Briefly, the average C_i–C_{i+1} segment length projected onto the bilayer normal (molecular lipid long axis) is obtained from the S^i_{CC} order parameter derived from S^i_{CD} using a recurrent mathematical expression. All C_i–C_{i+1} projected lengths are summed up all along the chain to obtain its average length.

(iv). X-Ray scattering experiments. The WAXS/SAXS data were measured at 298 K on a Rigaku FRX rotating anode X-ray generator at the copper wavelength (Kα, λ = 1.54 Å). The source is equipped with Osmic Varimax HF optics and a Dectris© Eiger 1 M detector on a 2θ arm of a Rigaku partial chi AFC11 goniometer. The samples were mounted in MicroLoops covered with microRT tubes from MiTeGen on a goniometer head under the cryostream nitrogen flux. The diffraction pattern corresponds to a 360° rotation along the phi axis (perpendicular to the direct beam with omega and chi axes at the 0 position) with an exposure time of 360 s at a detector distance of 114 mm. Data were integrated with CrysalisPro (Rigaku Oxford Diffraction, Ltd, Yarnton, Oxfordshire, England) with median filter and baseline correction.

The scattering factor q is calculated according to the equation $q(n) = 2\pi n/a_i$, where a_i is the lattice parameter with i = lamellar, hexagonal, cubic. For lamellar symmetry, $n^2 = h^2$, $k = l = 0$, for hexagonal, $n^2 = h^2 + k^2 + hk$, $l = 0$, $q(n) = 2\pi n/a_{\text{hexagonal}}2/\sqrt{3}$, for cubic $n^2 = h^2 + k^2 + l^2$. In the latter case the permitted combinations depend on the cubic phase of interest, for $Pm3n$, n^2 = 2, 4, 5, 6, 8, 10, 12, 13, ...[26] Calculations were performed using a home-made program written with MATLAB 2021a and compared to the experimental SAXS curves to obtain the best fit.

Results

Chemical synthesis

The *myo*-inositol-derived compound **5** is not commercially available and therefore a new practical synthesis had to be designed (Scheme 1). Thus, a per-benzylation of *myo*-inositol followed by a regioselective $TiCl_4$-mediated deprotection was initially planned, as described by Koto *et al.*[27] However, per-benzylation attempts only afforded a complex mixture of products (not described). Thus, a protected inositol derivative **5** with a free alcohol at position 1 was synthesized using a protection/deprotection sequence involving orthogonal protecting groups. First, hydroxyl groups at positions 1, 3 and 5 were protected as an orthobenzoate **1**, then positions 2, 4 and 6 were benzylated under standard conditions to give compound **2**. Position 5 was selectively opened by DIBAL-H, and the alcohol **3** was protected as benzyl ether **4**. Finally, the latter was opened with DIBAL-H to afford the desired compound **5** in 89% yield as a racemic mixture.

In order to rapidly access the archaeol synthesized in the literature from protected glycerol and phytanyl bromide[28] or phytanyl mesylate/triflate,[29,30] several options were investigated in this study in order to build this 1,2-diphytanylglycerol fragment. First, regioselective epoxide opening of protected glycidol derivatives by alcohols, as described by Abousalham *et al.*,[31] was unsuccessfully attempted. Then, a second pathway was investigated with phytyl bromide, starting from *rac*-solketal (Scheme 2).[32] Benzyl protection of the hydroxyl group of solketal followed by hydrolysis of the isopropylidene moiety provided diol **1** in 89–97% yields over two steps. Allylation of the

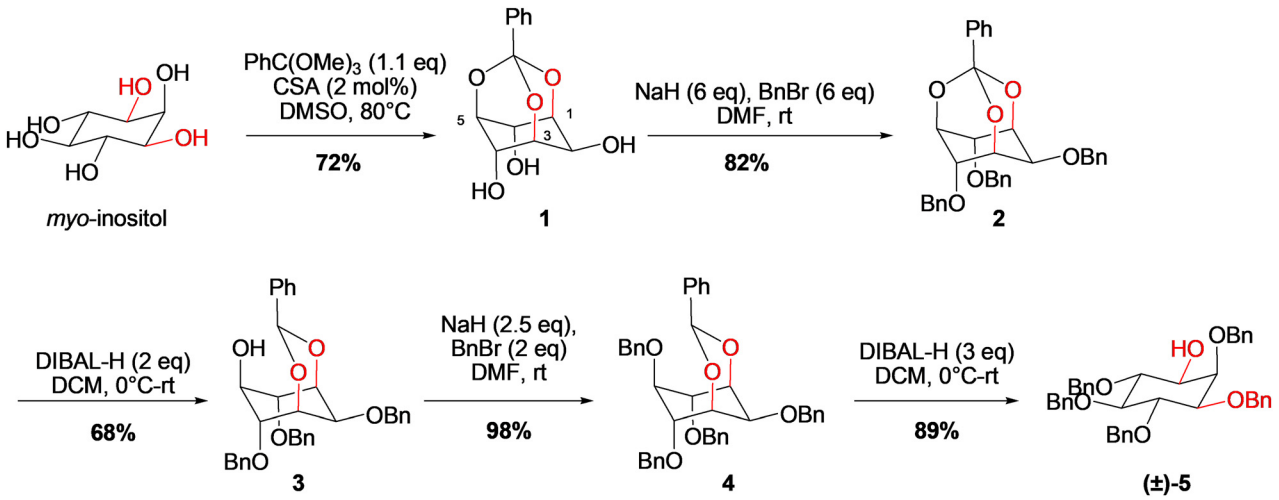

Scheme 1 Synthesis of inositol precursor for grafting.

Open Access Article. Published on 06 June 2023. Downloaded on 1/14/2026 1:25:04 AM.
This article is licensed under a Creative Commons Attribution-NonCommercial 3.0 Unported Licence.

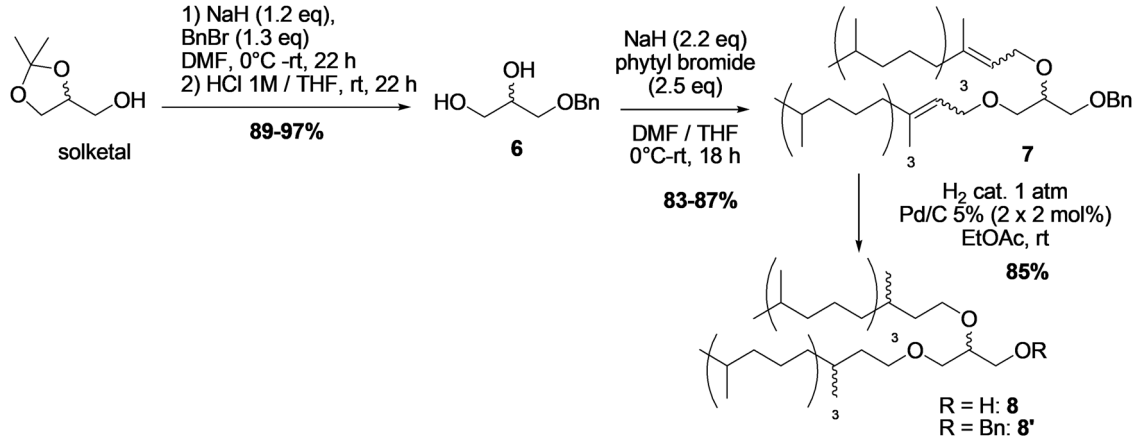

Scheme 2 Synthetic sequence for the archaeol **8** starting from solketal.

latter with phytyl bromide provided ether **7** in 83–87% yields (Scheme 2).

Because of the electrophilic activation of the allylic system, this pathway was preferred to the alkylation of **6** with electrophilic phytanyl bromide or triflate. Concerted olefin hydrogenation and benzyl deprotection of **7** afforded 1,2-diphytanylglycerol **8**. This step in particular required an important optimization (see ESI† on Protocols) due to an undesired hydrogenolytic cleavage of the allylic ether. With 2 mol% of Pd/C 5%, conversion was completed and the desired alcohol **8** was isolated in 30% yield along with tri-ether **8′** in 70% yield. When the catalyst was added in two portions (global loading of 4%), the substrate was converted into alcohol **8** in complete conversion of **8′** into **8**, with an isolated yield of 85%. Although hydrogenolytic cleavage of the allyl ether bond could not be entirely suppressed, this modification allowed scaling up of the procedure at 0.9–8 mmol scale in average to good yields.

Our next goal was to couple archaeol **8** with the phosphate moiety **9** and *myo*-inositol derivative **5** following a one-pot procedure described by Guanti *et al.*[33] (Scheme 3).

The strategy of coupling archaeol **8** and phosphoradiamidite **9** was considered, allowing the use of archaeol as the limiting agent. Thereby, phosphate ester **10** was obtained in 49% yield after these three steps.

The final step involves the release of the protecting groups (Scheme 4). Under standard conditions of catalytic hydrogenolysis with 10 mol% Pd/C, the choice of the solvent was critical due to the low solubility of the product. Further investigation highlighted a most effective procedure by using a water/THF (1/4) mixture. Under those conditions, the phosphatidylinositol derivative **11** was obtained in 79% yield.

Characterization by DLS

1,2-Diphytanylglycerol (archaeol) based lipids containing a phosphatidylinositol head group (derivative **11**) was then assessed for the ability to self-assemble into classical bilayer structures. Hereafter, derivative **11** will be referred to as DoPhPI. First, DoPhPI was mixed with different ratios of the commercially available and zwitterionic diphytanyl phosphatidylcholine (DoPhPC, Avanti Polar Lipids, ref. 999984) and solubilized in 50 mM Tris buffered D_2O pH 7.4. The mixtures of DoPhPI and DoPhPC (PI : PC) formed turbid solutions, which were then extruded through a 100 nm polycarbonate filter leading to the production of unilamellar vesicles (ULVs). The

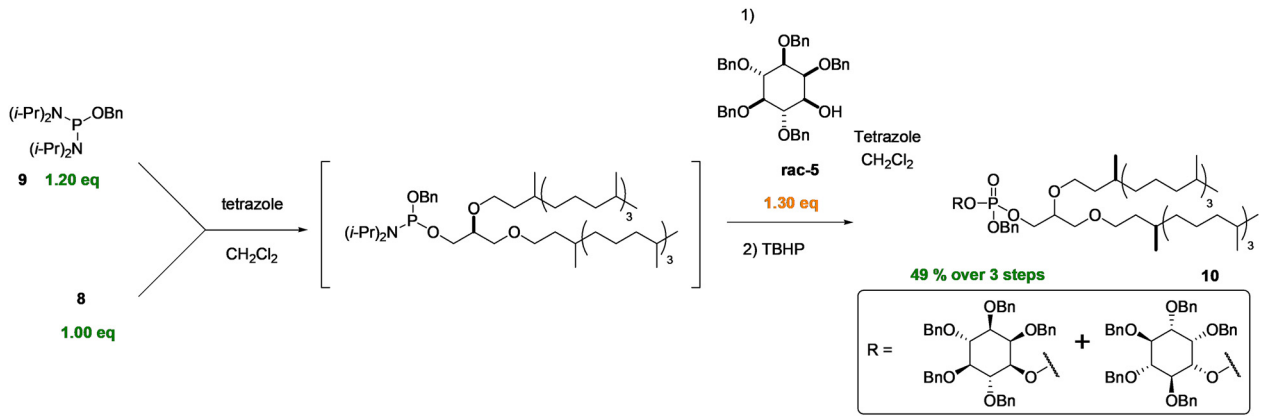

Scheme 3 Synthetic strategy for final grafting.

Open Access Article. Published on 06 June 2023. Downloaded on 1/14/2026 1:25:04 AM.
This article is licensed under a Creative Commons Attribution-NonCommercial 3.0 Unported Licence.

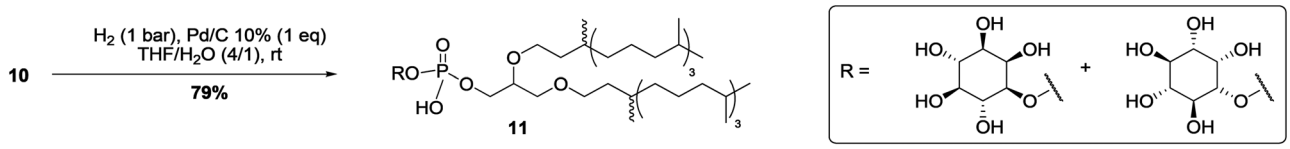

Scheme 4 Deprotection step affording the synthetic phospholipid.

DoPhPI alone did not solubilize completely at concentrations used for this experiment and was therefore not measured by DLS.

ULVs composed of DoPhPC, as well as 1 : 2, 1 : 1 and 2 : 1 mixtures of PI : PC were then probed using dynamic light scattering (Fig. 1, part a). The DLS data at 25 °C was fit using the method of cumulants to determine the rate of decay (see eqn (1)). The decay rate is proportional to the diffusion coefficient which could be used to determine the hydrodynamic radius of the vesicles calculated using the Stokes–Einstein relationship (see eqn (2)). Pure DoPhPC ULVs were found to have a hydrodynamic radius (R_h) of 73.8 ± 0.4 nm. The R_h of ULVs containing a mixture of DoPhPI and DoPhPC were found to be larger than that of DoPhPC alone and increased with an increase in the proportion of DoPhPI present from 82.2 ± 0.1 nm, to 85.7 ± 0.14 nm, to 106.3 ± 0.1 nm for DoPhPI : DoPhPC ratios of 1 : 2, 1 : 1 and 2 : 1 respectively (Fig. 1, part b). Temperature-dependent changes in vesicle R_h as well as polydispersity index (PDI) values at 25 °C between 0.17–0.19 for all samples can be found in Fig. S2 (ESI†).

Characterization by neutron diffraction

Next, the ability of DoPhPI containing membranes to form oriented bilayer structures was confirmed using neutron diffraction on the instrument D16 at the Institut Laue Langevin (ILL) Grenoble, France.[34] In typical bilayer forming systems, the hydration of lipid films by water vapor leads to the formation of stacks of lipid bilayers separated by layers of water. The repeating structure of these lipid multistacks, composed of the bilayer and the associated water layer, leads to the appearance of Bragg peaks in the diffraction data which can be used to characterize the bilayer structure (Fig. 2).[35,36]

Pure DoPhPI membrane as a function of temperature. DoPhPI was able to produce two sets of evenly spaced Bragg peaks which confirmed that these lipids form lamellar (bilayer) structures. The distance between the repeating units within the membrane stack (*d*-spacing) is inversely proportional to the distance between the Bragg peaks. The two sets of Bragg peaks indicate that two different lamellar phases, Phase 1 with a larger *d*-spacing and Phase 2 with a smaller *d*-spacing, are present (Fig. 2, part a).

At 25 °C, the *d*-spacing was found to be to 69.1 Å for Phase 1 and 48.7 Å for Phase 2. Diffraction data for DoPhPI was also measured at 40, 55, 70 and 85 °C. As the temperature increased there was a loss in intensity of the Phase 2 peaks with the *d*-spacing decreasing slightly to 47.8 Å, and Phase 2 was no longer seen at >40 °C. At least one Bragg peak was detected for Phase 1, at all temperatures tested (Fig. 2, part b). The peaks shifted to higher values of *q*, indicating a temperature dependent decrease in the *d*-spacing. The *d*-spacing of Phase 1 decreased to 65.6 Å at 40 °C, 64.0 Å at 55 °C, 62.2 Å at 70 °C, and 59.8 Å at 85 °C. The errors, based on the uncertainty of the peak position, are ±1.0 Å.

A similar temperature-dependent decrease in membrane *d*-spacing could be seen for the DoPhPI membrane at pressures of 10, 250, 500 and 1000 bar (Fig. S3, ESI†), which are the pressures relevant for piezophiles. Increasing pressure had the opposing effect, where increasing pressure led to an increase in

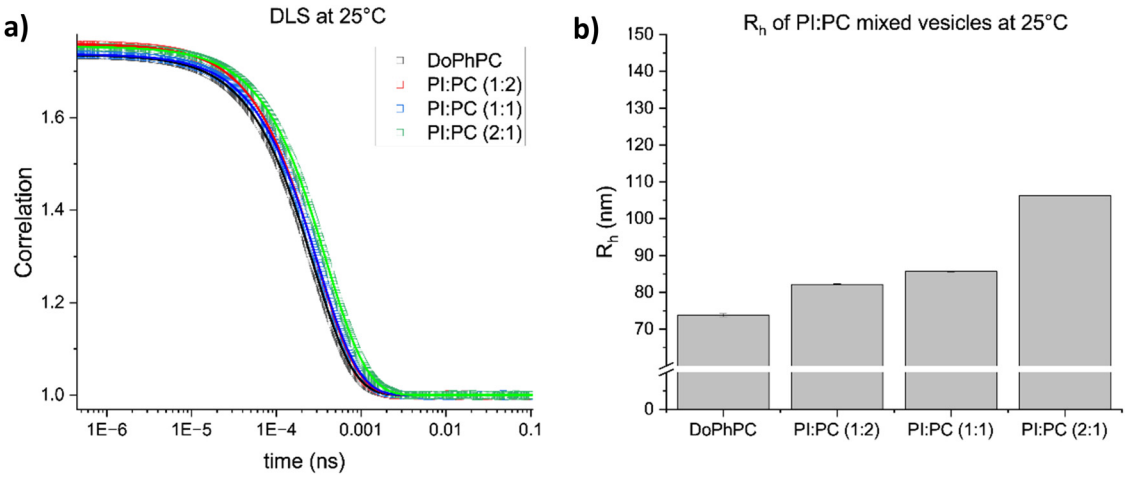

Fig. 1 Characterization of unilamellar vesicles (ULVs) containing DoPhPI by dynamic light scattering. (a) DLS correlation data at 25 °C. Data was fit using the method of cumulants. (b) Hydrodynamic radius (R_h) calculated from DLS data for ULVs containing DoPhPI.

Open Access Article. Published on 06 June 2023. Downloaded on 1/14/2026 1:25:04 AM.
This article is licensed under a Creative Commons Attribution-NonCommercial 3.0 Unported Licence.

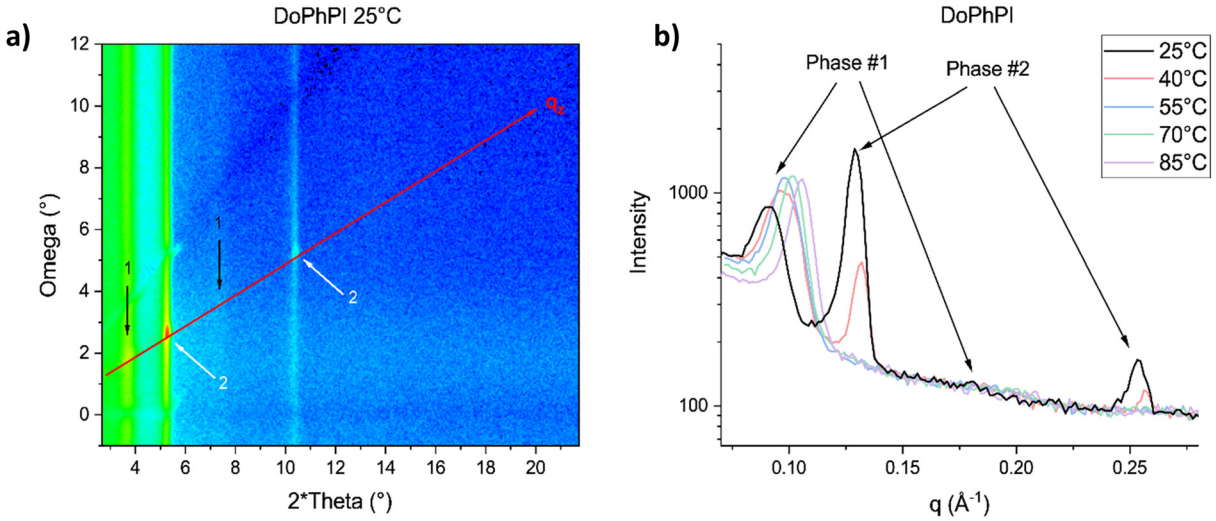

Fig. 2 Neutron diffraction from DoPhPI membrane multistacks at 100% D_2O contrast. (a) 2D diffractogram of DoPhPI membranes at 25 °C and ambient pressure in flat aluminium cell. Intensity profile was taken along the q_z axis. Two lamellar phases were seen. Peaks belonging to each phase are noted with either black arrows (Phase 1) or white arrows (Phase 2). (b) 1D diffractograms of DoPhPI membrane generated at 100% D_2O contrast with increasing temperature.

d-spacing, and also a stabilization of the DoPhPI Phase 2 (Table S1 and Fig. S4, ESI†).

Demixing in DoPhPI : DoPhPC (1 : 1) membrane. The diffraction signal for DoPhPI alone was relatively poor, producing a maximum of two Bragg peaks. In an attempt to improve the diffraction signal, we performed further studies using the DoPhPI mixed with DoPhPC in a 1 : 1 molar ratio at 25 °C and ambient pressure (see Fig. 3, part a and Fig. S5, ESI†). DoPhPC alone produced a single set of Bragg peaks with four orders of diffraction whose locations correspond to a *d*-spacing of 52.8 ± 0.8 Å. The PI : PC mixture produced two sets of Bragg peaks corresponding to two phases. PI : PC Phase 1, corresponded to a phase with a *d*-spacing of 73.5 ± 4.3 Å. PI : PC Phase 2, corresponded to a phase with a *d*-spacing of 51.5 ± 0.8 Å. The errors were evaluated from three contrast measurements.

Both DoPhPC and PI : PC Phase 2 had a sufficient number of Bragg peaks to calculate a neutron scattering length density (NSLD) plot to compare the two membranes.[37] The NSLD was plotted such that the center of the bilayer is located at 0 Å. The scattering minima at the center of the bilayer corresponds to the terminal methyl groups and the scattering density from the bilayer center to about ±15 Å corresponds to the hydrocarbon chains. The scattering density maxima found at around ±20 Å correspond to the polar region of the lipids including the glycerol and the polar head group and the minima at around ±27 Å correspond to the center of the water layer between adjacent bilayers. A comparison of the NSLD plots for the

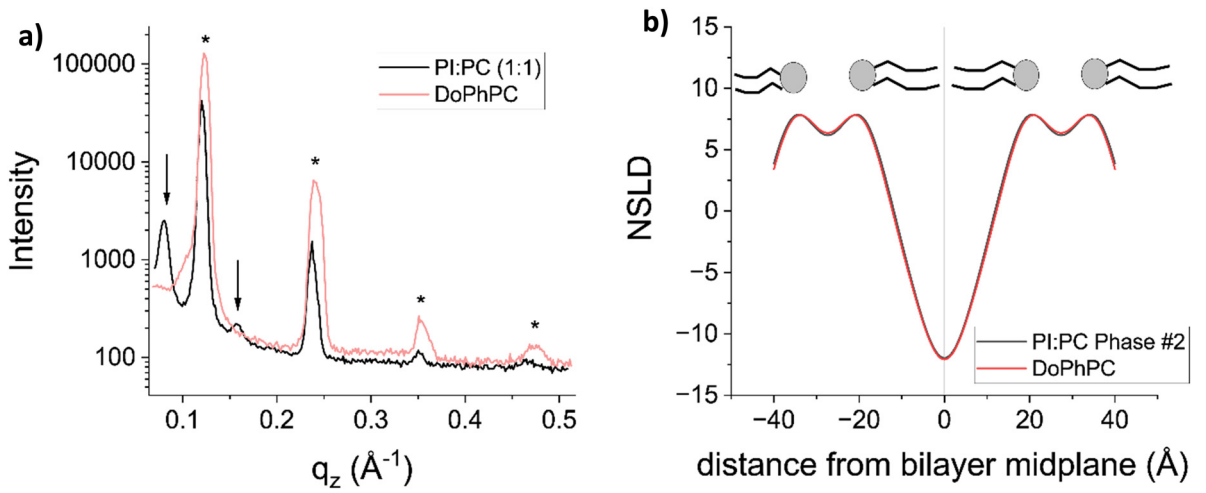

Fig. 3 Comparison of neutron diffraction for DoPhPC and PI : PC (1 : 1) membranes at 100% D_2O contrast. (a) 1D Diffractogram of PI : PC (1 : 1) compared with DoPhPC alone. Arrows are used to denote PI : PC Phase #1 and * to denote PI : PC Phase #2. (b) NSLD plot of DoPhPC me membrane (red) compared with Phase 2 of the PI : PC (1 : 1) membrane.

Open Access Article. Published on 06 June 2023. Downloaded on 1/14/2026 1:25:04 AM.
This article is licensed under a Creative Commons Attribution-NonCommercial 3.0 Unported Licence.

Table 1 *d*-spacing of DoPhPC, PI : PC (1 : 1), and DoPhPI membranes as a function of temperature measured in flat aluminum cell

T (°C)	DoPhPC	PI : PC phase 1	PI : PC phase 2	PI phase 1 (Å)	PI phase 2
25	52.8 ± 0.8	73.5 ± 4.3	51.5 ± 0.8	69.1	48.7
40	53.0 ± 1.0	69.4 ± 3.5	52.0 ± 1.6	65.6	47.8
55	53.5 ± 1.4	67.4 ± 2.7	n.d.	64.0	n.d.
70	54.0 ± 1.1	64.9 ± 2.8	n.d.	62.2	n.d.
85	54.7 ± 1.0	61.9 ± 2.2	n.d.	59.8	n.d.

PI : PC Phase 2 (black) and the DoPhPC membrane (red) are shown in Fig. 3, part b. The two NSLD plots are nearly identical. Neutron diffraction was measured for the PI : PC (1 : 1) membrane at temperatures up to 85 °C. PI : PC Phase 1 decreased in *d*-spacing as a function of temperature, similar to PI Phase 1. PI : PC Phase 2 was only detected at low temperatures (see Table 1).

Characterization by NMR

ssNMR of DoPhPC and DoPhPI mixtures in excess water. Wide line ^{31}P- and ^{2}H-NMR were performed as a function of temperature for DoPhPC and for equimolar mixtures of DoPhPC with DoPhPI (PI : PC). The temperature experiments were conducted as follows. After careful sample preparation at room temperature (*ca.* 60 min), the lipid dispersions were poured into the NMR tube (100 μL) and left in thermal equilibrium at 25 °C in the NMR spectrometer. ^{31}P- and ^{2}H-NMR were acquired (76 min) and the temperature was cooled to 5 °C. After a correct temperature reading in the probe, another equilibration time of 20 minutes was allowed before starting the acquisitions. Then the temperature was automatically increased by 5 °C, and a thermal equilibrium of 20 min was allowed after a correct temperature reading in the probe and ^{31}P- and ^{2}H-NMR were acquired. The same procedure was executed up to 67 °C (NMR setup limitation). The final experiment consisted of same acquisitions after returning to 25 °C. Fig. 4 shows selected ^{31}P-NMR spectra of the entire thermal variation (25 °C, 5 °C, 67 °C, 25 °C). All spectra are shown in Fig. S6 and S7 (ESI†) with the corresponding ^{2}H-NMR spectra.

The ^{31}P-NMR spectra of DoPhPC show an axially symmetric powder pattern (non-oriented sample) characteristic of a lamellar phase[23] with a chemical shielding anisotropy ($\Delta\sigma$) whose absolute value decreases monotonically with temperature from 50.0 to 43.8 ppm. The lamellar phase is also confirmed by ^{2}H-NMR (Fig. S6, ESI†). The spectra at 25 °C (initial, during the increase from low to high temperatures and back from 67 °C) are very similar, indicating that there is no hysteresis for the formation of the lamellar phase. The DoPhPC/DoPhPI system shows spectral features of lamellar plus cubic phases on starting the experiment or at low temperatures. One detects for the lamellar phase two axially asymmetric powder patterns with $\Delta\sigma$ = −48.7 and −61.1 ppm assignable respectively to the chemical shielding anisotropy of the PC and PI groups[38] at 25 °C. On increasing the temperature to 67 °C one detects spectral features characteristic of hexagonal ($\Delta\sigma$ = +19.4 ppm) plus cubic phases, the broad isotropic line (WHH = 300 Hz) dominating. Going back to 25 °C the system converts into a single broad isotropic line, *i.e.*, there is a clear thermal hysteresis.

Lipid phase determination and phase composition from ssNMR and SAXS. The NMR technique is quantitative and when detecting different spectral features that are in slow exchange, the area under each line corresponds to the molecular proportion of lipids engaged in this phase. ^{31}P-NMR spectra can be simulated to match the experimental and afford determination of the respective proportions (Fig. 5). The Table S2 (ESI†) compiles the results.

From this table, several graphs depicting the amount of each phase as a function of temperature can be plotted (Fig. 6). As a general comment it may be said that except for the DoPhPC the lamellar phase is not the dominant feature: hexagonal and cubic phases are detected. They determine the diagrams in the temperature range 5 to 67 °C, the hexagonal phase growing in importance with temperature.

We added 10 mol% $^{2}H_{31}$-DPPC to all systems to probe membrane internal dynamics as reported by the perdeuterated *sn*-2 palmitic chain (*vide infra*). The temperature variation as recorded from ^{2}H-ssNMR can be seen on Fig. S6 and S7 (ESI†). Comparison of simulations in ^{31}P-NMR and ^{2}H-NMR (Fig. 5) is very informative as ^{2}H-NMR reports only on DPPC partitioning. For instance, for the system DoPhPC/DoPhPI at 25 °C, the lamellar phase amounts 49%, the cubic, 51% whereas ^{2}H-DPPC is in lamellar phase for 90%. This clearly indicates that at this temperature the lamellar phase is enriched in PC species compared to the cubic that is rather a PI-rich phase.

WAXS/SAXS experiments were performed on NMR preparations by transferring the hydrated sample onto a Kapton loop, data collection was performed at 25 °C. After circular integration we obtain the classical Bragg peak representation of diffracted intensity as a function of $q = (4\pi \sin\theta/\lambda)$, Fig. S9 (ESI†). For lamellar phases, the diffracted peaks ratios scale as 1,2,3,4,5,6 ... as function of the Miller index *h*. For hexagonal lattices they scale as $(h^2 + k^2 + hk)^{1/2}$ with spacing of 1, $\sqrt{3}$, 2, $\sqrt{7}$, 3, $\sqrt{12}$, $\sqrt{14}$, ... For cubic phases they scale as $(h^2 + k^2 + l^2)^{1/2}$, for permitted combinations, with ratios spacings (*e.g.* for *Pm*3*n*) of $\sqrt{2}$, 2, $\sqrt{5}$, $\sqrt{6}$, $\sqrt{8}$, $\sqrt{10}$, $\sqrt{12}$, $\sqrt{13}$, ... Depending on samples investigated we indeed identified coexisting lamellar, hexagonal and cubic phases, at 25 °C, in complete agreement with ssNMR. The Table S3 (ESI†) reports the lattice parameters which are around 49–61 Å for lamellar, hexagonal and cubic phases. By parametrizing the scattering curves according to Braggs' spacings the best fit for the cubic phase was found for the *Pm*3*n* symmetry although other cubic symmetries may also explain the spacings (due to low resolution in WAXS/SAXS curves).

^{2}H-ssNMR for membrane dynamics and thickness. When there is only one lamellar phase in the system, calculation of the first spectral moment, M_1, allows to probe solid-ordered (so, also called lamellar gel) to liquid-disordered (ld, lamellar fluid) phase transitions. This is what is seen in Fig. 7a for MLV of $^{2}H_{31}$-DPPC. The sudden decrease of M_1 at around 37 °C indicates the sudden melting of palmitic chains at the

Open Access Article. Published on 06 June 2023. Downloaded on 1/14/2026 1:25:04 AM.
This article is licensed under a Creative Commons Attribution-NonCommercial 3.0 Unported Licence.

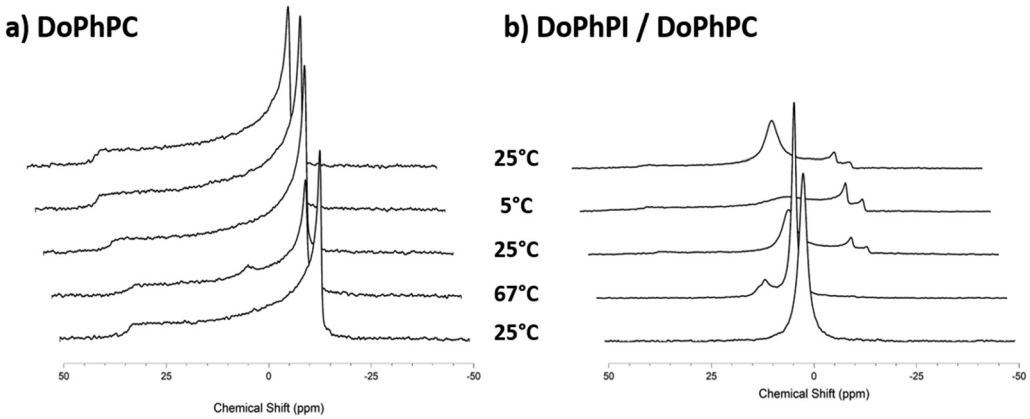

Fig. 4 Selected ^{31}P-ssNMR wide-line spectra of a temperature run of water dispersions of (a) DoPhPC, (b) DoPhPI : DoPhPC (1 : 1). $^{2}H_{31}$-DPPC is present as a probe at 0.1 : 1 mol to total lipids. Hydration is 82% (22 mg lipids/100 mg water). After careful sample preparation (see materials and methods), the samples were equilibrated to 25 °C (top spectrum), cooled to 5 °C for NMR acquisition (^{31}P-, middle top, and ^{2}H-NMR), and then stepwise increased to 67 °C (middle bottom), before descending to 25 °C where a final spectrum was acquired (bottom). 20 minutes were waited after temperature equilibrium before acquisition. Acquisition time at a given temperature is 42 min for ^{31}P-NMR and 34 min for ^{2}H-NMR representing a total time of 27 h for a full range of temperatures (14 temperatures). Acquisition parameters were kept constant for all experiments and are given in materials and methods.

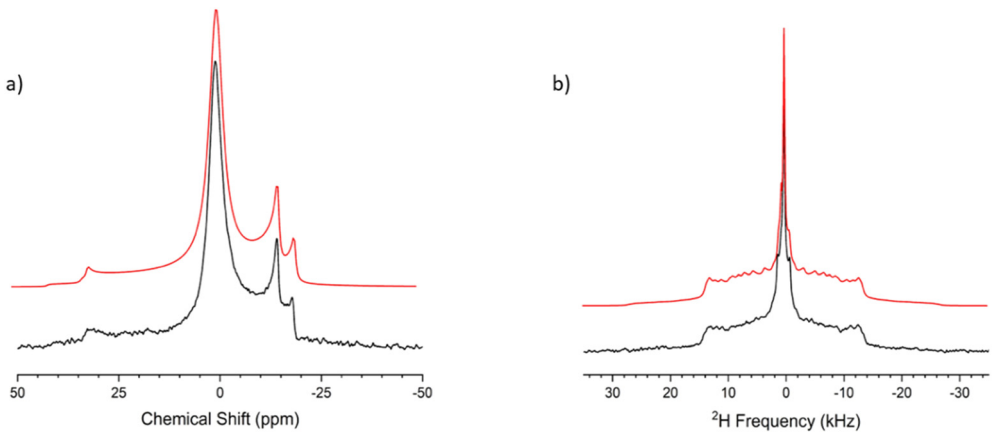

Fig. 5 Proportion membrane phases as determined from ^{31}P and ^{2}H spectral simulations. (a) black: experimental ^{31}P NMR spectrum of DoPhPI : DoPhPC (1 : 1 mol) at 25 °C, red: simulation L_α(PC) ($\Delta\sigma_1$= −48.7 ppm, 19%), L_α(PI) ($\Delta\sigma_2$ = −61.1 ppm, 30%), Cubic (51%). (b) black: experimental ^{2}H NMR spectrum of $^{2}H_{31}$-DPPC embedded in DoPhPI : DoPhPC (1 : 1 mol) at 25 °C, red: simulation L_α(PC) (15 labelled positions, 90%), Cubic (10%) (see Tables S4 and S5, ESI† for simulation parameters). Accuracy 5–10%.

$^{2}H_{31}$-DPPC so-lo transition temperature (3–4 degrees lower for perdeuterated chains than the usual T_m = 41 °C). When $^{2}H_{31}$-DPPC is embedded in DoPhPC in probe quantities, the so–lo transition is no longer detected, $^{2}H_{31}$-DPPC reports here on DoPhPC dynamics. The latter is still in the fluid lamellar phase at 5 °C and chain $^{2}H_{31}$-DPPC dynamics expressed with respect to the bilayer normal ($2S_{CDchain}$) is about 0.4 whereas it is 0.8 for pure $^{2}H_{31}$-DPPC; a value of 1.0 indicates the absence of chain isomerization, *i.e.* full rigidity. The ordering of the entire membrane appears lower than that of pure $^{2}H_{31}$-DPPC on the entire temperature variation (Fig. 7, part a). Detailed information on $^{2}H_{31}$-DPPC chain dynamics is obtained from simulations: the 15 ^{2}H-labelled positions are estimated from quadrupolar splitting measurements on experimental spectra and injected as first estimates in the calculation. Then, they are varied until a satisfactory superposition is obtained with the experimental spectrum. Fig. 7b brings details on $^{2}H_{31}$-DPPC ordering as a function of labelled carbon position on going from the interface (C2) towards the bilayer center (C16). The profiles are plotted for pure $^{2}H_{31}$-DPPC, $^{2}H_{31}$-DPPC in DoPhPC, in DoPhPC/DoPhPI (the lamellar phase only) at 40 °C. The profiles all show a plateau or order parameters for positions 2–8/10, and a quasi-linear decrease on going to position 16 in the center of the bilayer, a signature of lateral packing as already observed in lamellar phases.[23]

Order parameters can be used to calculate the average DPPC chain length.[25] This has been done in all cases where order parameters could be measured, *i.e.*, in lamellar fluid phase. Table S6 (ESI†) compiles the results. Values are much lower than the 19.6 Å of the fully extended palmitic chain as observed

Open Access Article. Published on 06 June 2023. Downloaded on 1/14/2026 1:25:04 AM.
This article is licensed under a Creative Commons Attribution-NonCommercial 3.0 Unported Licence.

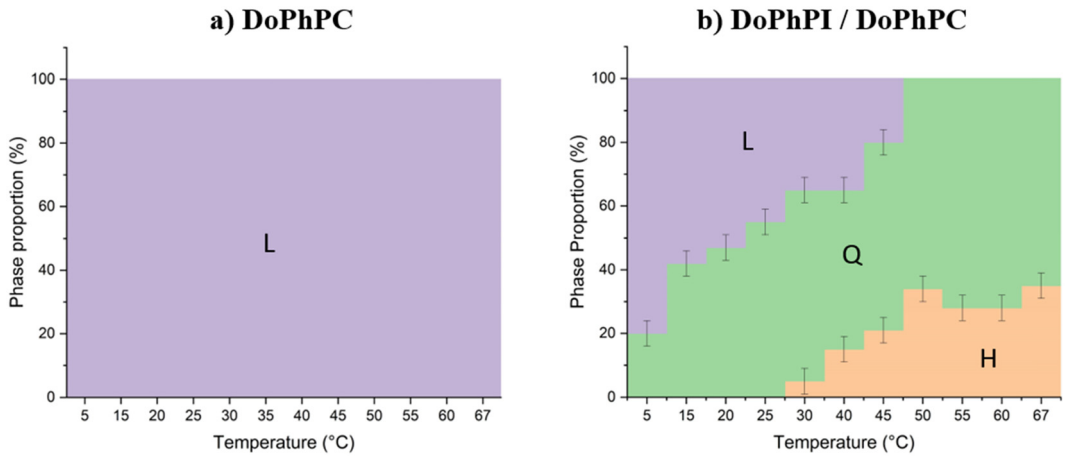

Fig. 6 Phase diagrams on increasing temperature (5–67 °C). (a) DoPhPC, (b) DoPhPI : DoPhPC (1 : 1). L = Lamellar L_α, H = Hexagonal type II phase, Q = cubic phase. Percentages are determined from spectral simulations of ^{31}P-NMR spectra. Accuracy 5–10%.

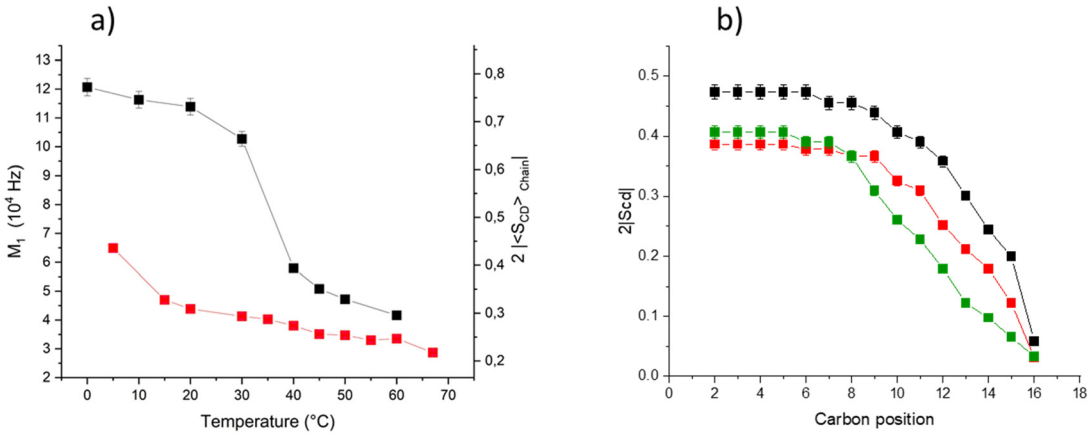

Fig. 7 Chain dynamics of DPPC, DoPhPC/DPPC, DoPhPC/DoPhPI/DPPC. (a) First spectral moment, M_1, and corresponding whole chain ordering, $2S_{CDchain}$, (double y-axis) as a function of temperature for $^2H_{31}$-DPPC (black squares) and DoPhPC/$^2H_{31}$-DPPC (red squares) water dispersions. $2S_{CDchain}$ is the absolute value of chain ordering projected onto the bilayer normal and is 1 for rigid systems and 0 for liquids.[1] Accuracy is 2.5%. (b) Absolute value of carbon-deuterium order parameter, S^k_{CD} as a function of labelled carbon position, k, on the sn-2 DPPC chain, for $^2H_{31}$-DPPC (black squares), DoPhPC/$^2H_{31}$-DPPC (red squares), DoPhPC/DoPhPI/$^2H_{31}$-DPPC (green squares), at 40 °C accuracy ± 0.002.

in rigid phases (L_C, $L_{\beta'}$): in all mixed systems one observes a huge reduction of 30–40%. As the accuracy in order parameters is 1%, that on chain length is ±0.1 Å, *i.e.*, very high. DPPC reports on lamellar phases and has average lengths of *ca.* 13 Å in phytanyl PC, PI, mixtures, at 40 °C, a value lower by about 1 Å compared to pure DPPC membranes at the same temperature. In all our systems, when there is a lamellar fluid phase one may estimate its bilayer thickness by making the approximation that it is close to twice the DPPC length. The latter is obtained by summing chain length and glycerophosphocholine head group, which has been estimated to be 7.0 ± 0.5 Å from neutron data.[25] This would lead to a DPPC length of 20.0 ± 0.5 Å in the lamellar phase of DoPhPC at 40 °C. It indicates that the bilayer thickness (approximated as twice the DPPC length) would be 40.0 ± 0.5 Å and would barely shrink to 39.4 ± 0.5 Å on going to 63 °C. Similar values can be obtained for other systems where lamellar phases are detected.

Dynamics of phytanyl chains from MAS ^{13}C-NMR. $^2H_{31}$-DPPC incorporated in lipid dispersions provides ordering information on the phase in which it is embedded (*vide supra*, hexagonal, lamellar). However, for the PI-containing system, we have observed a cubic phase that is featureless from the ^{2}H-NMR viewpoint (isotropic line) and from which no chain dynamics can be obtained from wide line spectra. We therefore utilized other NMR method to obtain complementary information on lipid dynamics: magic angle sample spinning (MAS) using INEPT and CP ^{13}C-NMR pulse sequences. This was applied to DoPhPC and DoPhPC : DoPhPI at 25 °C. INEPT and CP-MAS lead to high resolution natural abundance ^{13}C-NMR spectra by using the strong polarization transfer from protons to the low abundant ^{13}C nuclei (Fig. 8). The resonances of the CH_3, CH_2, CH and C groups in the phytanyl chains can easily be assigned and are significantly different from those of the corresponding groups in the saturated chains (see assignment in Fig. 8 and Table S7, ESI†). The choline head group shows 3

Open Access Article. Published on 06 June 2023. Downloaded on 1/14/2026 1:25:04 AM.
This article is licensed under a Creative Commons Attribution-NonCommercial 3.0 Unported Licence.

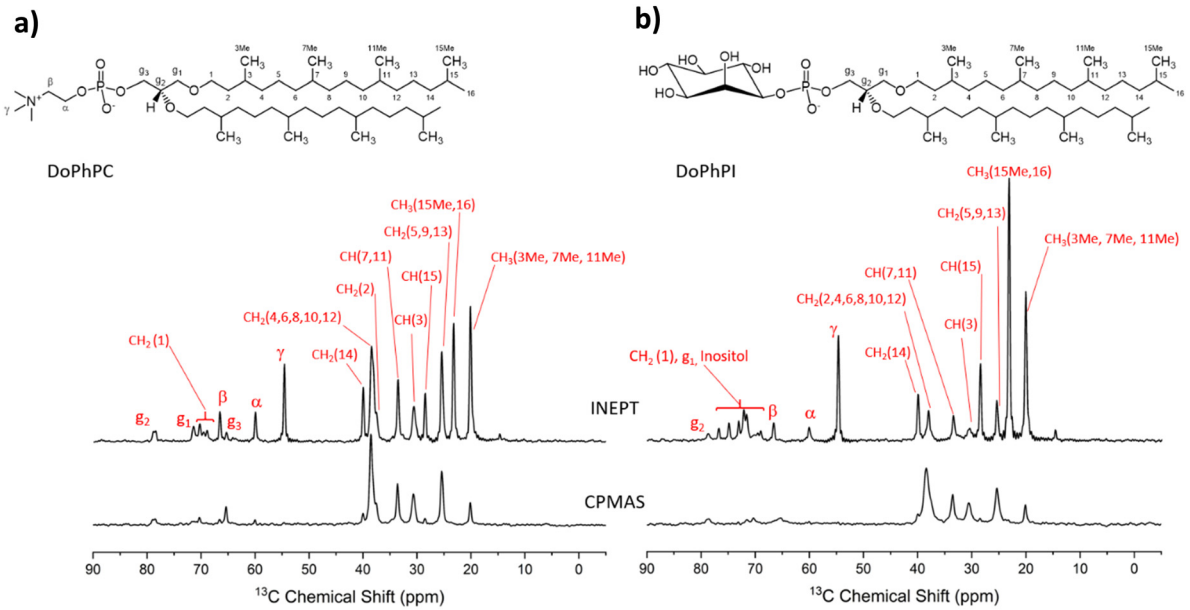

Fig. 8 Polarization enhanced ^{13}C-MAS NMR spectra (absolute intensity) of water dispersions of DoPhPC + 10% $^{2}H_{31}$-DPPC (a) and DoPhPC : DoPhPI (1 : 1) + 10% $^{2}H_{31}$-DPPC (b) using INEPT (middle) or CP (bottom) ^{1}H-polarization transfer at 25 °C. The upper part schematically represents the molecular structures of DoPhPC and DoPhPI with carbon numbering spectra by comparison of 1D and 2D experiments performed on pure DoPhPC solubilized in $CDCl_3$ (Fig. S8, ESI†). Acquisition parameters were kept constant for all experiments and are given in materials and methods.

resonances, α, β, γ (59.2, 66.9 and 54.9 ppm respectively). The PI head group has characteristic resonances of the inositol ring around 65–75 ppm.

The dynamical information is obtained by comparing resonance intensities obtained from the 2 techniques: INEPT refocuses the proton polarization of very mobile parts of the molecules, whereas CP does the same for the more rigid parts.[39–41] We performed both experiments using the same number of acquisitions. Spectra are shown in Fig. 8. Signals are observed both in INEPT and CP sequences indicating, not surprisingly, that there are mobile and more restricted parts in the lipid molecules. More specifically, for DoPhPC + 10% $^{2}H_{31}$-DPPC, one detects with the INEPT sequence choline ($-CH_2-CH_2-N^{+}(CH_3)_3$) resonances, common to both lipids, and the isopropyl (–CH(15), CH_3(15Me-16)) end group of the phytanyl chains. These resonances are only detected with the INEPT sequence meaning that theses molecular parts are very mobile. The other branched CH_3s[1,19,26] are also mobile as they dominate the INEPT spectrum. CH_2 and CH in chains, are mainly detected in CP experiments indicating a more restricted situation, as for glycerol resonances (g_1, g_2, g_3). A similar dynamical contrast is obtained for DoPhPC : DoPhPI + 10% $^{2}H_{31}$-DPPC. The very mobile choline, inositol and isopropyl group resonances are only detected in INEPT, whereas the CP resonances are mainly seen for glycerol, CH_2 and CH groups of phytanyl chains.

Discussion

(i) DLS

We were able to form unilamellar vesicles (ULVs) of diphytanyl membranes containing up to 2/3 DoPhPI, although we had difficulties with pure DoPhPI. Increasing the proportion of DoPhPI in PI : PC mixtures led to ULVs with a larger R_h. This is consistent with findings that in mixtures of DPPC and DPPI, the size of the vesicles increased with DPPI content.[42] An increase in vesicle radius is indicative of a decrease in the membrane curvature due to the PI head group. Lamellar phases have a curvature close to zero. Reducing curvature will eventually lead to non-lamellar phases such as cubic or hexagonal (type II) phase.

Extrusion through the 100 nm filter forces the formation of ULVs of given radius in DoPhPI containing membranes, but it cannot change the local bilayer structure which is defined by the lipid composition. DLS gives information on a distribution of particle sizes, but does not permit for distinguishing the organization or the type of lipid phase within the particles, which might be present anyway.

(ii) Neutron diffraction

DoPhPI alone is capable of assembling into lamellar structures when hydrated on a solid support. Interestingly, DoPhPI assembled into two different lamellar phases with the *d*-spacing of PI Phase 1 ≫ PI Phase 2 by ∼20 Å at 25 °C. The exact nature of these phases is not known but the very large difference in spacing likely indicates a change in the thickness of the water layer between the two phases. In addition to hydration, the orientation of the head group or the racemic nature of the synthesized DoPhPI lipid could also impact the different behavior of the two phases.

Mixtures of PI : PC also assemble into two different lamellar phase at 25 °C. The NSLD plots of PI : PC Phase 2 and DoPhPC are nearly identical indicating that PI : PC Phase 2 is likely

Open Access Article. Published on 06 June 2023. Downloaded on 1/14/2026 1:25:04 AM. This article is licensed under a Creative Commons Attribution-NonCommercial 3.0 Unported Licence.

composed almost entirely of DoPhPC. If PI : PC Phase 2 is a PC-rich phase then PI : PC Phase 1 is therefore PI-rich. This is consistent with the finding that PI : PC Phase 1 had a much larger repeat spacing than DoPhPC and in particular with PI Phase 1. The PI-rich phase (PI : PC Phase 1) consistently had a *d*-spacing which was larger than that of the largest phase seen for pure DoPhPI, suggesting that this phase, while PI-rich, contains some DoPhPC. The quantity of DoPhPC within the PI-rich phase is sufficient to influence the lamellar repeat spacing of the phase.

The PI : PC membrane exhibited phase coexistence, in this case, due to demixing between the two lipids. Not only did the diffraction data show the coexistence of PC-rich and a PI-rich phases, but it also gave information about the lateral organization of these phases. In addition to the Bragg peaks found along the q_z axis, satellite peaks could be seen both above and below the q_z axis indicating organization within the membrane plane (Fig. S5, ESI†). Analysis of the location of these satellite peaks was then used to calculate a repeating distance in the plane of the bilayer d_x = 321.2 ± 3.8 Å.

Increasing the temperature above 40 °C, led to a loss of both PI Phase 2 and PI : PC Phase 2. The *d*-spacing of PI Phase 1 decreased significantly with increasing temperature. Similarly the PI-rich phase of the PI : PC membrane also experience a decrease in *d*-spacing with temperature. These changes are most likely the result of dehydration of the membrane stack. The behavior of PI containing membrane phases is quite different from DoPhPC which shows a slight increase in *d*-spacing with increasing temperature, consistent with findings for other PC lipids.[43–45] Increases in the *d*-spacing of other PC lipids at full hydration have also been reported. In these examples, the increase was attributed to a rise in the thickness of the water layers, which was caused by larger membrane fluctuations at higher temperature drawing additional water into the lamellar phasew.[46] The differences between DoPhPI and DoPhPC lipid behavior highlights the importance of the polar head group in the assembly of lipid structures.

Only lamellar phases were seen by neutron diffraction. The preparation of the lipids on a solid support may promote lamellar phases over non-lamellar phases which could otherwise be observed in multilamellar vesicles by ssNMR or SAXS (*vide infra*).

(iii) NMR & SAXS

Our work on fully hydrated mixtures of synthetic archaeal lipids shines a new light on the assembly and dynamics of such systems. In accordance with DLS, neutrons and SAXS we found that DoPhPC forms lamellar phases whereas addition of DoPhPI promotes the appearance of cubic and hexagonal phases, the latter being observed at high temperature. The dynamics of the membrane interior is very high due to the branched phytanyl chains and does not very much on large temperature scales. These results will be discussed below and their biological relevance in the context of the first appearance of life on earth will be commented on.

DoPhPI promotes non-lamellar phases. Our experiments clearly demonstrate that non-lamellar phases are observed for DoPhPI lipids added in equimolar amounts to DoPhPC. This is in accordance with neutrons scattering that found coexisting lamellar spacings probably due to the geometry of the stacked layers of the neutrons setup. The ssNMR and SAXS samples had no such constrains and non-lamellar phases can freely be formed. By increasing the temperature, the cubic phase is first observed and then the hexagonal type II phase appears for a further thermal increase. Coexistence is observed at ambient temperatures in the NMR time scale, that is in our case greater than the ms. The SAXS technique also detects several phases which means that they are in thermal equilibrium on even longer time scales (minutes). Lattice parameters (Table S3, ESI†) are of *ca.* 50–60 Å. The bilayer thickness has been estimated by NMR to be around 40 Å indicating that the water layer in the different structures is *ca.* 10–20 Å. The appearance of hexagonal phases at high temperature could be understood as a formation at the expense of cubic phases, the system undergoing a kind of dehydration, the trapped water being ejected to the bulk water reservoir. This could be explained by a slightly smaller lattice parameter for the hexagonal phases, as observed, the small spacing of *ca.* 47 Å being also observed with neutrons. This dehydration phenomenon could also explain a slight irreversibility of some systems when the sample temperature is decreased from high temperatures. The induction of non-lamellar phases is not surprising, *per se*, as the area of the two phytanyl chains (*ca.* 100–120 Å^2)[47] is much larger than that of head groups of PC and PG (50–65 Å^2), PS (40–60 Å^2), PI (> PC) or PE (40–50 Å^2).[47–50] Hence the tendency to induce inverted curved structures such as H_{II} or *Pm*3*n* is not surprising.

Non-lamellar phases were not seen by DLS or neutron diffraction but the preparation of lipids differ between techniques. Neutron diffraction experiments are performed on a solid support which may promote organization into lamellar phases. Extrusion of samples for DLS may also promote lamellar phases. DLS results showed that DoPhPI promoted a larger vesicle radius – indicating a more negative membrane curvature. The formation of cubic followed by hexagonal phases seen by NMR is also related to a decrease in membrane curvature.

Dynamics of lipids in lamellar, hexagonal and cubic phases. Lipid chain dynamics was approached *via* deuterium and carbon-13 NMR. Local dynamics promoted by intramolecular (bond isomerization) or molecular motions (lipid wobbling in a cone) is first reported by deuterium NMR of labelled DPPC embedded as a probe in all the systems. Very interestingly, the palmitoyl chains are still very fluid at ambient (20 °C) temperatures indicating that phytanyl chains impose important chain disordering. The DPPC chains are even more disordered than in their pure fluid phase. This is confirmed by looking directly at phytanyl chain dynamics using ^{13}C-NMR. All branched methyl groups are very dynamic (free rotation) and the end isopropyl group is also very mobile. CH and CH_2 groups of the phytanyl chains and of the glycerol backbone have a more restricted mobility although their low intensity in the CP-MAS experiments indicates a high degree of disorder,[40,41] in agreement with deuterium NMR of $^2H_{31}$-DPPC. Interestingly, in situation of mixed phases, *e.g.*, PC/PI (lamellar + hexagonal + cubic),

Open Access Article. Published on 06 June 2023. Downloaded on 1/14/2026 1:25:04 AM.
This article is licensed under a Creative Commons Attribution-NonCommercial 3.0 Unported Licence.

the intensity is even lower suggesting an increased mobility of the phytanyl chains when a non-lamellar phase is present. This is due to the fact that chain dynamics in non-lamellar phases is greater that in lamellar phases. It is again understandable, the volume of the chains is greater due to the curved interface and therefore less lateral packing is exerted in the chains, freeing the fragments to reorient further.

Conclusions

A convenient synthesis of archaeal lipids including inositol derived lipids has been reported using archaeol which was further converted using the phosphoramidite methodology to phosphodiester derivatives, allowing for the first time the synthesis of the main phospholipid of hyperthermophilic Archaea. Structural characterization of DoPhPI showed that this lipid presents some original characteristics and is able to form lamellar (bilayer) structures upon extrusion of water dispersions or when oriented on plates. Very interestingly membranes containing DoPhPI show a preference for more negative membrane curvatures which can lead to the formation of cubic and hexagonal phases when the water dispersions are not constrained by the experimental set up, as has been seen for bilayer membranes containing squalane in their midplane.[51] Phytanyl chains are also very dynamic and are capable to impose their dynamics even in the presence of long saturated chains. The ability of squalane to relax phytanyl chain frustration inside the bilayer has been proposed as one of the mechanism by which it increases membrane stability and functionality in the archaeal membrane. Here, the high dynamics of the phytanyl chains and the observation of very curved interfaces at high temperatures observed for DoPhPI appears very similar, and might provide an exceptional membrane plasticity and could be seen as another adaptation route for hyperthermophilic Archaea to adapt to extreme conditions of temperature and pressure.

Author contributions

Conceptualization, E. J. D., F. P., J. P.; methodology, E. J. D., B. K., L. S., B. D.; formal analysis, J. R., J. G. L., A. G., M. S. C.; investigation, J. R., J. G. L., M. S. C.; resources, J. P.; data curation, J. R., J. G. L., A. G.; writing—original draft preparation, A. G., E. J. D., J. G. L., F. P., J. R., J. P.; writing—review and editing, all authors; supervision, F. P., J. P.; project administration, E. J. D., F. P., J. P.; funding acquisition, J. P. All authors have read and agreed to the published version of the manuscript.

Conflicts of interest

There are no conflicts to declare.

Acknowledgements

We thank P. Oger for the fruitful discussions. The ILL is acknowledged for the allocation of beamtime on D16. This work was supported by the French National Research Agency programme ANR 17-CE11-0012-01. Roland Winter and Simon Krieger are thanked for preliminary SAXS experiments.

Notes and references

1 J. G. Beck, D. Mathieu, C. Loudet, S. Buchoux and E. J. Dufourc, Plant sterols in "rafts": a better way to regulate membrane thermal shocks, *FASEB J.*, 2007, **21**, 1714–1723.
2 P. L. Chong, Archaebacterial bipolar tetraether lipids: Physico-chemical and membrane properties, *Chem. Phys. Lipids*, 2010, **163**, 253–265.
3 A. Caforio and A. J. M. Driessen, Archaeal phospholipids: Structural properties and biosynthesis, *Biochim. Biophys. Acta, Mol. Cell Biol. Lipids*, 2017, **1862**, 1325–1339.
4 Y. Koga and H. Morii, Biosynthesis of ether-type polar lipids in archaea and evolutionary considerations, *Microbiol. Mol. Biol. Rev.*, 2007, **71**, 97–120.
5 P. M. Oger and A. Cario, Adaptation of the membrane in Archaea, *Biophys. Chem.*, 2013, **183**, 42–56.
6 A. Cario, V. Grossi, P. Schaeffer and P. M. Oger, Membrane homeoviscous adaptation in the piezo-hyperthermophilic archaeon Thermococcus barophilus, *Front. Microbiol.*, 2015, **6**, 1152.
7 *eLS*, John Wiley & Sons, ed. G. D. Sprott, 2011.
8 M. F. Siliakus, J. van der Oost and S. W. M. Kengen, Adaptations of archaeal and bacterial membranes to variations in temperature, pH and pressure, *Extremophiles*, 2017, **21**, 651–670.
9 K. P. Law, W. He, J. Tao and C. Zhang, A Novel Approach to Characterize the Lipidome of Marine Archaeon Nitrosopumilus maritimus by Ion Mobility Mass Spectrometry, *Front. Microbiol.*, 2021, **12**, 735878.
10 M. Tourte, V. Kuentz, P. Schaeffer, V. Grossi, A. Cario and P. M. Oger, Novel Intact Polar and Core Lipid Compositions in the Pyrococcus Model Species, P. furiosus and P. yayanosii, Reveal the Largest Lipid Diversity Amongst Thermococcales, *Biomolecules*, 2020, **10**, 830.
11 P. Schleger, B. Alefeld, J. Barthelemy, G. Ehlers, B. Farago, P. Giraud, C. Hayes, A. Kollmar, C. Lartigue, F. Mezei and D. Richter, The long-wavelength neutron spin-echo spectrometer IN15 at the Institut Laue-Langevin, *Phys. B*, 1997, **241–243**, 164–165.
12 P. Schleger, G. Ehlers, A. Kollmar, B. Alefeld, J. F. Barthelemy, H. Casalta, B. Farago, P. Giraud, C. Hayes, C. Lartigue, F. Mezei and D. Richter, The sub-neV resolution NSE spectrometer IN15 at the Institute Laue–Langevin, *Phys. B*, 1999, **1–2**, 49–55.
13 B. J. Frisken, Revisiting the method of cumulants for the analysis of dynamic light-scattering data, *Appl. Opt.*, 2001, **40**, 4087–4091.
14 V. Cristiglio, B. Giroud, L. Didier and B. Demé, D16 is back to business: More neutrons, more space, more fun, *Neutron News*, 2015, **26**, 22–24.
15 J. Peters, M. Golub, B. Demé, J. Gonthier, C. Payre, J. Maurice, R. Sadykov and E. Lelièvre-Berna, New pressure

Open Access Article. Published on 06 June 2023. Downloaded on 1/14/2026 1:25:04 AM.
This article is licensed under a Creative Commons Attribution-NonCommercial 3.0 Unported Licence.

cells for membrane layers and systems in solutions up to 100 °C, *J. Neutron Res.*, 2018, **20**, 3–12.

16 E. Lelièvre-Berna, B. Demé, J. Gonthier, J. P. Gonzales, J. Maurice, Y. Memphis, C. Payre, P. Oger, J. Peters and S. Vial, 700 MPa sample stick for studying liquid samples or solid-gas reactions down to 1.8 K and up to 550 K, *J. Neutron Res.*, 2017, **19**, 77–84.

17 M. Rance and R. A. Byrd, Obtaining high-fidelity powder spectra in anisotropic media: Phase-cycled Hahn echo spectroscopy, *J. Magn. Reson.*, 1983, **52**, 221–240.

18 J. H. Davis, K. R. Jeffrey, M. Bloom, M. I. Valic and T. P. Higgs, Quadrupolar echo deuteron magnetic resonance spectroscopy in ordered hydrocarbon chains, *Chem. Phys. Lett.*, 1976, **42**, 390–394.

19 A. Pines, M. G. Gibby and J. S. Waugh, Proton-Enhanced Nuclear Induction Spectroscopy. A Method for High Resolution NMR of Dilute Spins in Solids, *J. Chem. Phys.*, 1972, **56**, 1776–1777.

20 G. A. Morris and R. Freeman, Enhancement of nuclear magnetic resonance signals by polarization transfer, *J. Am. Chem. Soc.*, 1979, **101**, 760–762.

21 J. H. Davis, Deuterium Magnetic-Resonance Study Of The Gel And Liquid-Crystalline Phases Of Dipalmitoyl Phosphatidylcholine, *Biophys. J.*, 1979, **27**, 339–358.

22 T. Pott and E. J. Dufourc, Action of Melittin on the DPPC-Cholesterol Liquid-Ordered Phase-A Solid-State 2H-NMR and P-31-NMR Study, *Biophys. J.*, 1995, **68**, 965–977.

23 J. H. Davis, The Description of Membrane Lipid Conformation, Order and Dynamics by 2H-NMR, *Biochem. Biophys. Acta*, 1983, **737**, 117–171.

24 S. Buchoux, J. Lai-Kee-Him, M. Garnier, P. Tsan, F. Besson, A. Brisson and E. J. Dufourc, Surfactin-triggered small vesicle formation of negatively charged membranes: A novel membrane-lysis mechanism, *Biophys. J.*, 2008, **95**, 3840–3849.

25 J. P. Douliez, A. Leonard and E. J. Dufourc, Restatement of Order Parameters in Biomembranes - Calculation of C-C Bond Order Parameters from C-D Quadrupolar Splittings, *Biophys. J.*, 1995, **68**, 1727–1739.

26 M. I. Aroyo, *International Tables For Crystallography, Volume A: Space-Group Symmetry*, Wiley, Chester, United Kingdom, 2016.

27 S. Koto, M. Hirooka, T. Yoshida, K. Takenaka, C. Asai, T. Nagamitsu, H. Sakuma, M. Sakurai, S. Masuzawa, M. Komiya, T. Sato, S. Zen, K. Yago and F. Tomonaga, Syntheses of penta-O-benzyl-myo-inositols, O-beta-L-arabinosyl-(1 -> 2)-*sn*-myo-inositol, O-alpha-D-galactosyl-(1 -> 3)-*sn*-myo-inositol, and O-alpha-D-galactosyl-(1- >6)-O-alpha-D-galactosyl-(1 -> 3)-*sn*-myo-inositol, *Bull. Chem. Soc. Jpn.*, 2000, **73**, 2521–2529.

28 V. Atanasov, P. P. Atanasova, I. K. Vockenroth, N. Knorr and I. Köper, A molecular toolkit for highly insulating tethered bilayer lipid membranes on various substrates, *Bioconjug. Chem.*, 2006, **17**, 631–637.

29 T. Aoki and C. D. Poulter, Archaebacterial isoprenoids. Synthesis of 2,3-di-O-phytanyl-*sn-glycerol* and its 1,2-isomer, *J. Org. Chem.*, 1985, **50**, 5634–5636.

30 T. Eguchi, K. Arakawa, T. Terachi and K. Kakinuma, Total Synthesis of Archaeal 36-Membered Macrocyclic Diether Lipid, *J. Org. Chem.*, 1997, **62**, 1924–1933.

31 M. El Alaoui, L. Soulère, A. Noiriel, F. Popowycz, A. Khatib, Y. Queneau and A. Abousalham, A continuous spectrophotometric assay that distinguishes between phospholipase A1 and A2 activities, *J. Lipid Res.*, 2016, **57**, 1589–1597.

32 C. A. A. van Boeckel, P. Westerduin and J. H. van Boom, Synthesis of 2,3-di-O-phytanyl-1-O-[glucosyl (galactosyl)-β(1 → 6) -mannosyl-α(1 → 2)-glucosyl-α (1 → 1)]-*sn-glycerol*. Purple membrane glycolipids, *Tetrahedron Lett.*, 1981, **22**, 2819–2822.

33 G. Guanti, L. Banfi, A. Basso, L. Bondanza, G. Guglieri, K. Powles and R. Riva, Optimized synthesis of phosphatidylserine, *Amino Acids*, 2010, **39**, 367–373.

34 V. Cristiglio, B. Giroud, L. Didier and B. Demé, D16 is back to business: more neutrons, more space, more fun, *Neutron News*, 2015, **26**, 22–24.

35 G. Fragneto, Neutrons and model membranes, *Eur. Phys. J. Special Topics*, 2012, **213**, 327–342.

36 J. F. Nagle and S. Tristram-Nagle, Structure of lipid bilayers, *Biochim. Biophys. Acta*, 2000, **1469**, 159–195.

37 D. L. Worcester and N. P. Franks, Structural analysis of hydrated egg lecithin and cholesterol bilayers II. Neutron diffraction, *J. Mol. Biol.*, 1976, **3**, 359–378.

38 V. Zhendre, A. Grelard, M. Garnier-Lhomme, S. Buchoux, B. Larijani and E. J. Dufourc, Key Role of Polyphosphoinositides in Dynamics of Fusogenic Nuclear Membrane Vesicles, *PLoS One*, 2011, **6**, e23859.

39 A. Nowacka, P. C. Mohr, J. Norrman, R. W. Martin and D. Topgaard, Polarization Transfer Solid-State NMR for Studying Surfactant Phase Behavior, *Langmuir*, 2010, **26**, 16848–16856.

40 E. Morvan, N. Taib-Maamar, A. Grelard, A. Loquet and E. J. Dufourc, Bio-membranes: Picosecond to second dynamics and plasticity as deciphered by solid state NMR, *Biochim. Biophys. Acta, Biomembr.*, 2022, 184097, DOI: **10.1016/j.bbamem.2022.184097**.

41 E. Morvan, N. Taib-Maamar, A. Grelard, A. Loquet and E. J. Dufourc, Dynamic sorting of mobile and rigid molecules in biomembranes by magic-angle spinning 13C-NMR, *Anal. Chem.*, 2023, **95**, 3596–3605.

42 K. Hammond, M. D. Reboiras, I. G. Lyle and M. N. Jones, Characterisation of phosphatidylcholine/phosphatidylinositol sonicated vesicles. Effects of phospholipid composition on vesicle size, *Biochim. Biophys. Acta*, 1984, **774**, 19–25.

43 S. A. Simon, S. Advani and T. J. McIntosh, Temperature dependence of the repulsive pressure between phosphatidylcholine bilayers, *Biophys. J.*, 1995, **69**, 1473–1483.

44 N. Kucerka, M. P. Nieh and J. Katsaras, Fluid phase lipid areas and bilayer thicknesses of commonly used phosphatidylcholines as a function of temperature, *Biochim. Biophys. Acta*, 2011, **1808**, 2761–2771.

45 N. Kucerka, S. Tristram-Nagle and J. F. Nagle, Structure of Fully Hydrated Fluid Phase Lipid Bilayers with Monounsaturated Chains, *J. Membr. Biol.*, 2006, **208**, 193–202.

 This journal is © the Owner Societies 2023

Open Access Article. Published on 06 June 2023. Downloaded on 1/14/2026 1:25:04 AM.
This article is licensed under a Creative Commons Attribution-NonCommercial 3.0 Unported Licence.

46 S. C. Costigan, P. J. Booth and R. H. Templer, Estimations of lipid bilayer geometry in fluid lamellar phases, *Biochim. Biophys. Acta*, 2000, **1468**, 41–54.
47 K. Yamauchi, K. Doi and M. Kinoshita, Archaebacterial lipid models: Stable liposomes from 1-alkyl-2-phytanyl-*sn*-glycero-3-phosphocholines, *Biochim. Biophys. Acta-Biomembr.*, 1996, **1283**, 163–169.
48 R. A. Demel, F. Paltauf and H. Hauser, Monolayer Characteristics And Thermal-Behavior Of Natural And Synthetic Phosphatidylserines, *Biochemistry*, 1987, **26**, 8659–8665.
49 H. Mansour, D. S. Wang, C. S. Chen and G. Zografi, Comparison of bilayer and monolayer properties of phospholipid systems containing dipalmitoylphosphatidylglycerol and dipalmitoylphosphatidylinositol, *Langmuir*, 2001, **17**, 6622–6632.
50 D. Marsh, *Handbook of lipid Bilayers*, CRC Press, Boca Raton, 2nd edn, 2013.
51 M. Salvador-Castell, M. Golub, N. Erwin, B. Demé, N. J. Brooks, R. Winter, J. Peters and P. M. Oger, Characterisation of a synthetic Archeal membrane reveals a possible new adaptation route to extreme conditions, *Commun. Biol.*, 2021, **4**, 653.